Identifying Higher-Order Interactions in Wave Time-Series

Kevin Ewans
MetOcean Research Ltd.,
New Plymouth 4310, New Zealand
e-mail: kevin.ewans@mrl.nz

Marios Christou
Department of Civil & Environmental Engineering,
Imperial College,
London SW7 2AZ, UK
e-mail: marios.christou@imperial.ac.uk

Suzana Ilic
Lancaster Environment Centre,
Lancaster University,
Lancaster LA1 4YQ, UK
e-mail: s.illic@lancaster.ac.uk

Philip Jonathan
Shell Research Ltd., UK,
Mathematics & Statistics,
Lancaster University,
Manchester M22 0RR, UK
e-mail: philip.jonathan@shell.com

Reliable design and reanalysis of coastal and offshore structures require, among other things, characterization of extreme crest elevation corresponding to long return periods. Extreme crests typically correspond to focused wave events enhanced by wave–wave interactions of different orders—third-order, four-wave interactions dominating in deep water (Janssen, P. A. E. M., 2003, "Nonlinear Four-Wave Interactions and Freak Waves," J. Phys. Oceanogr., 33(4), pp. 863–884). Higher-order spectral (HOS) analysis can be used to identify wave–wave interactions in time-series of water surface elevation; trispectral analysis is needed to detect third-order, four-wave interactions. Four-wave interactions between Fourier components can involve interactions of the type where $f_1+f_2+f_3=f_4$ and where $f_1+f_2=f_3+f_4$, resulting in two definitions of the trispectrum—the T- and V-trispectrum (with corresponding tricoherences), respectively. It is shown that the T-tricoherence is capable of detecting phase-locked four-wave interactions of the type $f_4=f_1+f_2+f_3$ when these are simulated with simple sinusoids, but such interactions were not detected in HOS model simulations and field data. It is also found that high V-tricoherence levels are detected at frequencies at which four-wave interactions of the type $f_1+f_2=f_3+f_4$ are expected, but these may simply indicate combinations of independent pairs of Fourier components that happen to satisfy the frequency relationship. Preliminary analysis shows that using a cumulant-based trispectrum (Kravtchenko-Berejnoi, V., Lefeuvre, F., Krasnosel'skikh, V. V., and Lagoutte, D., 1995, "On the Use of Tricoherent Analysis to Detect Nonlinear Wave–Wave Interactions," Signal Process., 42(3), pp. 291–309) may improve identification of wave–wave interactions. These results highlight that caution needs to be exercised in interpreting trispectra in terms of specific four-wave interactions occurring in sea states and further research is needed to establish whether this is in fact possible in practice. [DOI: 10.1115/1.4047930]

Keywords: ocean waves and associated statistics, offshore safety and reliability, probability and spectral wave modeling, higher-order spectral analysis

Introduction

The power spectrum, based on Fourier analysis, has been widely used as a tool to study ocean wind waves by scientists and engineers alike, since its introduction for this purpose around 1950. Barber et al. [1] published the first wave spectra, and Pierson and Marks [2] introduced power spectrum analysis to ocean wave data analysis, following techniques pioneered by Tukey [3]. The wave power spectrum provides a frequency representation of the surface elevation that can be used to identify the most energetic Fourier components for engineering applications, and it is fundamental in numerical wave prediction models.

The power spectrum provides a complete description of the frequency content of the sea surface if it consists of a linear superposition of statistically independent free waves. However, insight into higher-order effects, such as those resulting from three and four-wave interactions, which for example may lead to the occurrence of an extreme crest, require more sophisticated analyses techniques—viz., higher-order spectral (HOS) analysis.

Higher-order spectral analysis is formulated in a general way from the definition of cumulants [4]. Accordingly, the power spectrum is the Fourier transform of the second-order cumulant, the bispectrum is the Fourier transform of the third-order cumulant, the trispectrum is the Fourier transform of the fourth-order cumulants, and in general, the kth-order polyspectrum is the Fourier transform of the $(k+1)$th-order cumulant.

The bispectrum is a function of two frequencies and provides an estimate of the degree of coupling between wave components at the two frequencies and a third; it is therefore an appropriate tool to investigate triad interactions in a sea state. Hasselmann et al. [5] was the first to use the bispectrum to examine such second-order interactions in sea states; other examples include Elgar and Guza [6], Cherneva and Guedes Soares [7], and Toffoli et al. [8].

The trispectrum is a function of three frequencies and provides an estimate of the degree of coupling between wave components at the three frequencies and a fourth, thus being appropriate for investigating quadruplet interactions in sea states. Examples of the use of the trispectrum to investigate quadruplet interactions in sea states include Chandran et al. [9], Elgar et al. [10], and Aubourg et al. [11].

Four-wave interactions between Fourier components can involve interactions of the type where $f_1+f_2+f_3=f_4$ and where $f_1+f_2=f_3+f_4$, resulting in two definitions of the trispectrum, depending on which of the two interactions is of interest. The first, appropriate for interactions of the type $f_1+f_2+f_3=f_4$, in a time-series, $x(t)$, is given by

$$T(f_1,f_2,f_3)=X(f_1)X(f_2)X(f_3)X^*(f_4)$$

where $f_4=f_1+f_2+f_3$, and for example, $X(f)$ is the Fourier transform of $x(t)$, $X^*(f)$ is the complex conjugate of $X(f)$.

The second, appropriate for interactions of the type $f_1+f_2=f_3+f_4$, is given by

$$V(f_1,f_2,f_3)=X(f_1)X(f_2)X^*(f_3)X^*(f_4)$$

where $f_4=f_1+f_2-f_3$.

It is useful to normalize the higher-order spectra, to enable the degree of nonlinear interaction to be quantified. Several normalization definitions can be found in the literature. Chandran et al. [9] defines two, both extensions of normalizations of bispectra—one based on that used by Haubrich [12], and one based on that used by Kim and Powers [13]. Aubourg et al. [11] used a normalization

Contributed by the Ocean, Offshore, and Arctic Engineering Division of ASME for publication in the Journal of Offshore Mechanics and Arctic Engineering. Manuscript received March 29, 2020; final manuscript received June 27, 2020; published online August 24, 2020. Assoc. Editor: Nilanjan Saha.

based on power spectra. The squared magnitude of the bispectrum and trispectrum are often referred to as bicoherence and tricoherence, respectively. Thus, for example, the tricoherence, for interactions of the type $f_1+f_2+f_3=f_4$, based on the Kim and Powers [13] normalization is defined as

$$t^2(f_1,f_2,f_3)=|\mathcal{T}(f_1,f_2,f_3)|^2$$

where

$$\mathcal{T}(f_1,f_2,f_3)=\frac{E[T(f_1,f_2,f_3)]}{\sqrt{E[|X(f_1)X(f_2)X(f_3)|^2]E[|X(f_4)|^2]}}$$

where $E[\cdot]$ is the expectation operator.

It can be shown that $0\le t^2\le 1$ [9], which permits the interpretation that the tricoherence is a measure of the fraction of the total product of powers at the frequency quartet, (f_1, f_2, f_3, f_4) that are phase-coupled.

In terms of the second trispectrum definition, for interactions of the type $f_1+f_2=f_3+f_4$

$$v^2(f_1,f_2,f_3)=|\mathcal{V}(f_1,f_2,f_3)|^2$$

where

$$\mathcal{V}(f_1,f_2,f_3)=\frac{E[V(f_1,f_2,f_3)]}{\sqrt{E[|X(f_1)X(f_2)X(f_3)|^2]E[|(f_4)|^2]}}$$

Hinich and Wolinsky [14] favor a statistical definition for the normalization and argue that the normalization based on Kim and Powers [13] can give misleading results for large sample sizes for which high spectral resolution is possible and used. Nevertheless, the Kim and Powers [13] definition provides for a convenient interpretation, and records of ocean waves are typically not long enough to allow sufficient reliability in Fourier estimates at very high frequency resolution.

In this paper, we compute the t^2 and v^2 tricoherence, which we refer to as T- and V-tricoherence estimates for a number of signals. We begin with various combinations of sine waves, to gather evidence on how the tricoherence estimators might be interpreted in terms of four-wave interactions. This experience is then used to evaluate the tricoherence estimates for numerical simulations using a nonlinear wave model, laboratory measurements of a steep sea state that would be expected to involve higher-order wave–wave interactions, and the field measurement recording that includes the famous Draupner wave that is believed to result from higher-order effects. The immediately following section provides a brief description of the spectral estimation technique.

Spectral Estimation Method

Spectral analysis of the digital time-series signals, $x(t_i)$, are processed following the Welch [15] method. That is, $x(t_i)$ is divided into L segments, each of length N, a power of 2. $X(f_i)$ for each segment are estimated using the fast Fourier transform algorithm. The required quantities—e.g., $X(f_i)X(f_j)X(f_k)$, for $X(f_1)X(f_2)X(f_3)$ and $X(f_i)X(f_j)X(f_k)X^*(f_l)$ for $X(f_1)X(f_2)X(f_3)X^*(f_4)$—are estimated for each segment and the expected values estimated from the average of each quantity over all L segments.

Each segment is windowed with a Hanning window (see for example, Ref. [16]) and may be half-overlapped with adjacent segments, to improve the spectral reliability. Accordingly, we have half-overlapped segments in the case of the simulated HOS data and the measured data, to maximize reliability, but we have not overlapped the segments in the case of the sine waves for which reliability is not an issue.

To mitigate spurious large estimates of tricoherence corresponding to occurrences of near-zero values of the denominator in the tricoherence expression, a regularization parameter of size 0.01 times the numerator is added to the denominator throughout. This introduces a bias of 1% at the peak tricoherence.

Tricoherence of Sinusoids

Insight into the behavior of the trispectrum is obtained by examining the trispectrum of a signal $y(t)$ consisting of four sinusoids immersed in a background of Gaussian noise. A theoretical outline for the observed results is given in the Appendix

$$y_1(t)=\sum_{i=1}^{5}\mathrm{a}_i\sin(2\pi f_i t+\phi_i)$$

$$y_2(t)=N(0,\ \mathrm{var}(y_1(t)))$$

$$y(t)=y_1(t)+y_2(t)$$

where $a_1=a_2=a_3=1$; $f_1=0.0521$ Hz, $f_2=0.1437$ Hz, $f_3=0.0710$ Hz; $\phi_1=0$, $\phi_2=\pi/16$, $\phi_3=\pi/3$.

We vary the frequency and phase of the fourth and fifth sinusoids, a_4, f_4, ϕ_4, a_5, f_5, and ϕ_5, for a number of test case as tabulated in Table 1, but in each case $f_5=f_4$. $U(0, 2\pi)$ in Table 1 denotes the uniform distribution on the interval $[0, 2\pi)$.

Test Case SIN1. In this case, the frequency of the fourth sinusoid is the sum of the frequencies of the other three sinusoids, and its phase is the sum of the phases of the other sinusoids

$$f_4=f_1+f_2+f_3=0.2668\ \mathrm{Hz}$$

$$\phi_4=\phi_1+\phi_2+\phi_3$$

This case therefore corresponds to four-wave interactions in which the fourth wave is forced by and phase-locked to the other three.

The T-tricoherence is a function of three independent frequency variables and so difficult to display. Here, we take slices through the axis of one frequency variable to show results in two-dimensional, and we label the axes as f_1, f_2, and f_3. Accordingly, an image of the T-tricoherence, for the slice $f_3=f_1$; i.e., $T(f_1, f_2, f_3=f_1)$, is given in Fig. 1 on log10 scale. The vertical and horizontal dashed lines correspond to the four frequencies, both in the same order as the vertical lines are labelled. The image is symmetric about the diagonal dashed line. The dark regions corresponds to f_4 being outside the positive frequency range (top right region of the plot) or when the tricoherence value is less than 0.001. Considering the region for $f_1<f_2$ (below the diagonal dashed line), the maximum (circled) tricoherence of 0.688 occurs at the triplet $f_1=f_2$, $f_2=f_3$, $f_3=f_1$; i.e., the triplet (f_2, f_3, f_1). The relatively large value of the tricoherence in this case reflects strong phase coupling at this combination of frequencies, as we might expect. Corresponding peaks at the other permutations of the f_1, f_2, and f_3 triplet are also observed when similarly plotted.

The corresponding V-tricoherence is given in Fig. 2. The dark regions are as described for Fig. 1. The maximum of 0.877 can be seen to occur at the triplet (f_1, f_1, f_1), and the vertical and horizontal ridge of high values (at $f_1=f_1, f_2=f_1$) correspond to cases satisfying $f_1+f_2=f_3+f_4$. The tricoherence is higher at values of f_1 and f_2 equal to any of the frequencies of the four sinusoids; these are referred to as "trivial" cases for the V-tricoherence.

Table 1 Fourth and fifth sinusoid parameters for the five test cases

Case	a_4	f_4	ϕ_4	a_5	ϕ_5
SIN1	1	$f_1+f_2+f_3$	$\phi_1+\phi_2+\phi_3$	0	0
SIN2	1	$f_1+f_2+f_3$	$U(0, 2\pi)$	0	0
SIN3	0.5	$f_1+f_2+f_3$	$U(0, 2\pi)$	0.5	$\phi_1+\phi_2+\phi_3$
SIN4	1	$f_1+f_2-f_3$	$\phi_1+\phi_2+\phi_3$	0	0
SIN5	1	$f_1+f_2-f_3$	$U(0, 2\pi)$	0	0

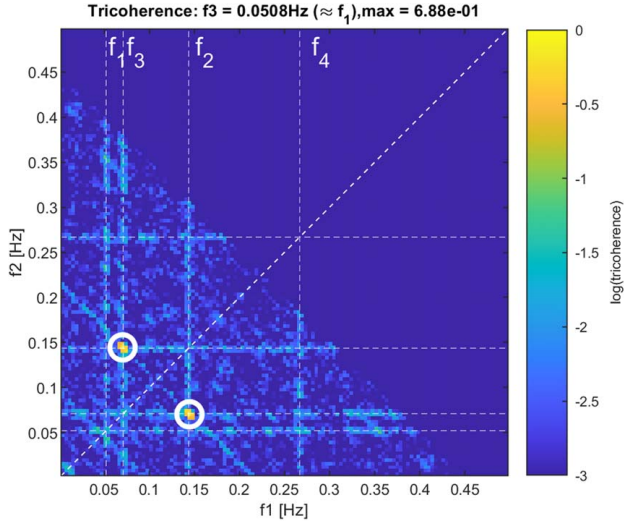

Fig. 1 Image of T-tricoherence for $f_3 = 0.0508$ Hz for case SIN1

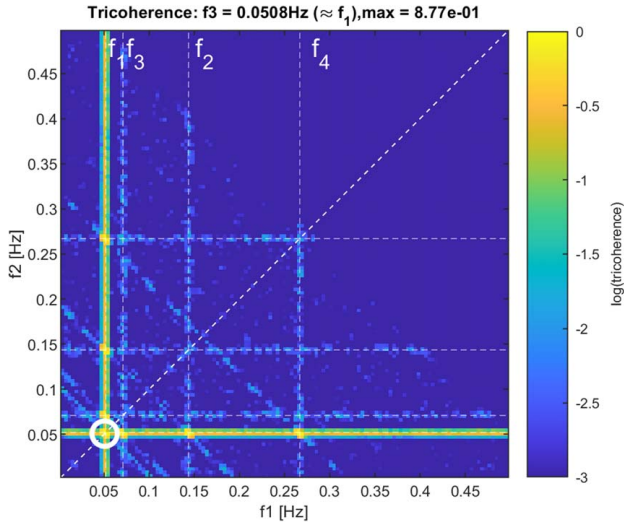

Fig. 2 Image of V-tricoherence for $f_3 = 0.0508$ Hz for case SIN1

An overall picture of the tricoherence is achieved by computing the tricoherence maximum for a given value of f_3 (over all choices of f_1 and f_2) and plotting these maxima as a function of f_3. Such f_3 maxima slices for both definitions of the tricoherence are plotted in Fig. 3. Both show maxima at the frequencies f_1, f_2, and f_3, but the V-tricoherence shows an additional peak at f_4, which is not present in the T-tricoherence. The V-tricoherence also shows a higher background level of noise, probably associated with fortuitous matching of the condition $f_1 + f_2 = f_3 + f_4$.

Test Case SIN2. In this case, the signal is the same as for case SIN1, except that a random phase is assigned to the fourth sinusoid. This is achieved by selecting a different random phase for ϕ_4 at the beginning of each segment. The phase for each segment is drawn from a uniform distribution over $[0, 2\pi)$.

The f_3 axis slice maxima for the two tricoherence definitions are given in Fig. 4. The V-tricoherence is essentially unchanged (from Fig. 3) by the introduction of the random phase. The T-tricoherence is however now absent of the peaks evident in the phase-locked case. Apparently, the V-tricoherence gives the same result, irrespective of whether or not the phases are locked or not. On the other hand, the T-tricoherence requires that the phases are locked to be detected above the noise floor.

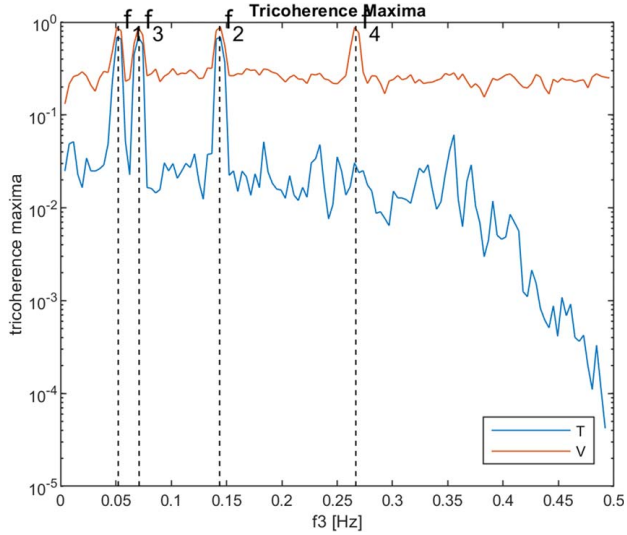

Fig. 3 f_3 slice maxima for the T and V-tricoherence estimates, for the phase-locked sinusoidal signal (SIN1)

Test Case SIN3. We also examined the effect of a partially phase-coupled fourth component by adding a fifth sinusoid, such that $f_5 = f_4$, $a_5 = 0.5$, $\phi_5 = \phi_1 + \phi_2 + \phi_3$, and setting $a_4 = 0.5$, effectively involving a fourth component split equally between a phase-coupled part and a random phase part. The f_3 axis slice maxima for the two tricoherence definitions are given in Fig. 5. The V-tricoherence curve is unchanged from that in Fig. 3. The T-tricoherence curve is similar that in Fig. 3—the level of the background noise is the same, but the peaks are reduced to about half the level of those in Fig. 3. This confirms that partially phase-coupled components can be detected by the T-tricoherence and also that the amount of phase-coupling at a given combination of frequencies will be indicated.

Test Case SIN4. In this case, the signal is the same as for case SIN1, except for the definition of f_4. This case corresponds to the four-wave interaction $f_1 + f_2 = f_3 + f_4$ with locked phase.

The f_3 axis slice maxima for the two tricoherence definitions are given in Fig. 6. Apart from a shift in the location of fourth sinusoid

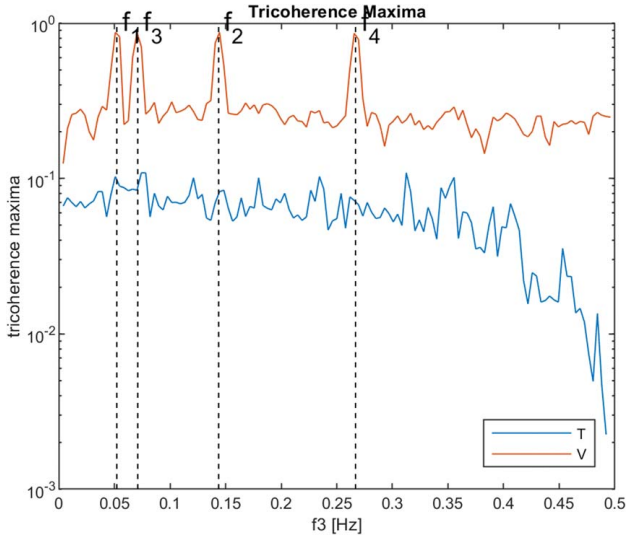

Fig. 4 f_3 slice maxima for the T and V-tricoherence estimates, for the sinusoidal signal for which the fourth component is assigned a random phase for each segment (case SIN2)

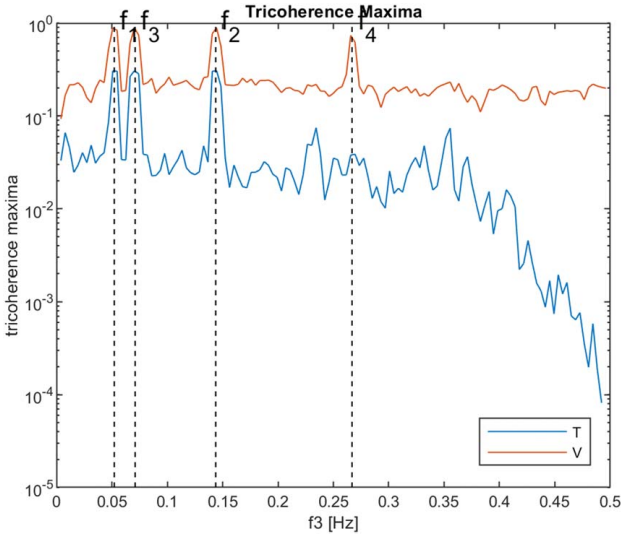

Fig. 5 f_3 **slice maxima for the T and V-tricoherence estimates, for the partially phase-locked sinusoidal signal (case SIN3)**

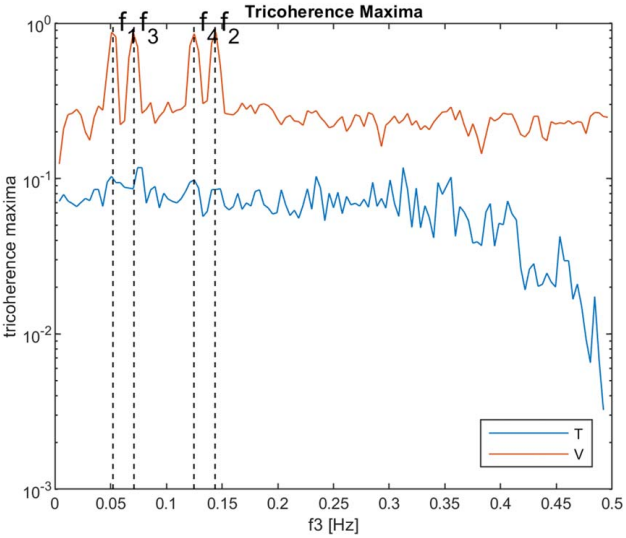

Fig. 6 f_3 **slice maxima for the T and V-tricoherence estimates, for the sinusoidal signal of case SIN4**

in the V-tricoherence, the spectra in Fig. 6 are the same as those in Fig. 4. However, as the combination of sinusoids do not satisfy the condition $f_4 = f_1 + f_2 + f_3$, none of the sinusoids is detected by the T-tricoherence definition.

The image of the V-tricoherence, for the slice $f_3 = f_1$; i.e., $V(f_1, f_2, f_3 = f_1)$, is given in Fig. 7. The high levels associated with the trivial cases of the same type as those identified in Fig. 2 are seen in Fig. 7, but a significant peak can be noted for the Fourier frequencies 0.0508 Hz ($\approx f_1$), 0.0703 Hz ($\approx f_3$), and 0.125 Hz ($\approx f_4$), which is a triplet that satisfies the interaction condition for SIN4. This suggests that it is possible to identify four-wave interactions of the SIN4 type with the V-tricoherence, when the frequencies of the four interacting components are different.

Test Case SIN5. In this case, the signal is the same as for Case SIN4, except that a random phase is assigned to the fourth sinusoid, as for case 2. The results for this case are contrary to those for case 3, showing that the V-tricoherence is sensitive to whether the phases of the components are phase-locked or not, for the case $f_1 + f_2 = f_3 + f_4$.

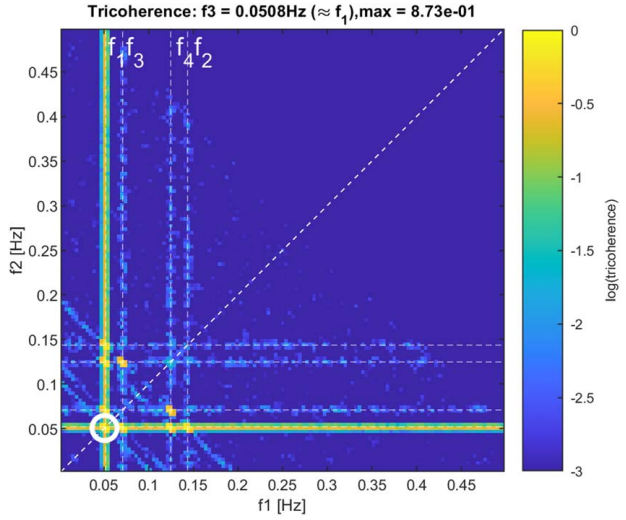

Fig. 7 Image of V-tricoherence for $f_3 = 0.0508$ **Hz for case SIN4**

The image of the V-tricoherence, for the slice $f_3 = f_1$; i.e., $V(f_1, f_2, f_3 = f_1)$, is given in Fig. 8. By comparison with Fig. 7, it is notable that the peak at the Fourier frequencies 0.0508 Hz ($\approx f_1$), 0.0703 Hz ($\approx f_3$), and 0.125 Hz ($\approx f_4$) is not present in Fig. 8, indicating a lack of capability of the V-tricoherence to detect four-wave interactions of SIN5 type—i.e., where one of the components has random phase.

Higher-Order Spectral Model Signal

Numerical simulations were performed using the HOS model that was developed in the LHEEA Laboratory at Ecole Centrale Nantes, France. HOS is a computationally efficient, open-source model that can accurately simulate the nonlinear behavior of surface waves propagating in the ocean [17,18]. All simulations used the HOS-ocean program to simulate unidirectional wave fields. The length of the computational domain L_x was set to $42\lambda_p$ (where λ_p is the wave length corresponding to the peak period T_p), the simulations were run for $235T_p$ with a Dommermuth initialization of duration $10T_p$ and n equal to 4. The HOS order was set to 5, and 10^{-7} was used for tolerance of the Runge–Kutta Cash–Karp time marching scheme. HOS runs of order 3 would have been sufficient to produce the effects that the trispectrum is expected to identify, but real sea states are not limited to order 3, and we expect HOS

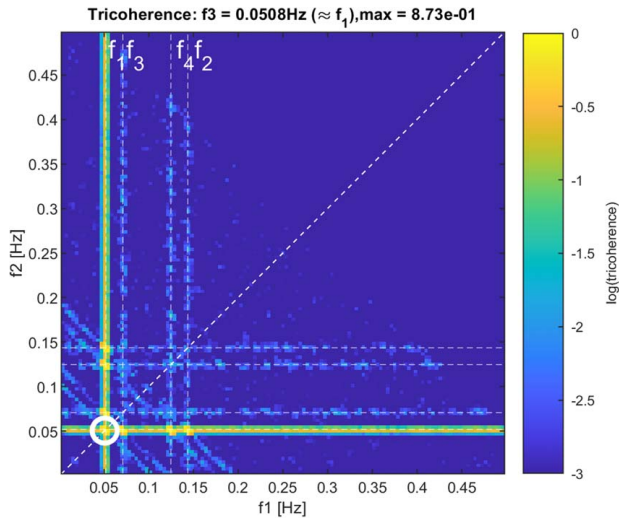

Fig. 8 Image of V-tricoherence for $f_3 = 0.0508$ **Hz for case SIN5**

Table 2 Key parameters for the HOS-ocean unidirectional simulations using the JONSWAP spectrum

Case	H_s (m)	T_p (s)	γ	d (m)
HOS1	5.0	16	2.5	Infinite
HOS2	10.0	16	2.5	Infinite
HOS3	12.5	16	2.5	Infinite
HOS4	15.0	16	2.5	Infinite
HOS5	15.0	16	2.5	65
HOS6	15.0	16	10.0	125

Note: H_s is the significant wave height, T_p is the peak period, γ is the peak enhancement factor, and d is the water depth.

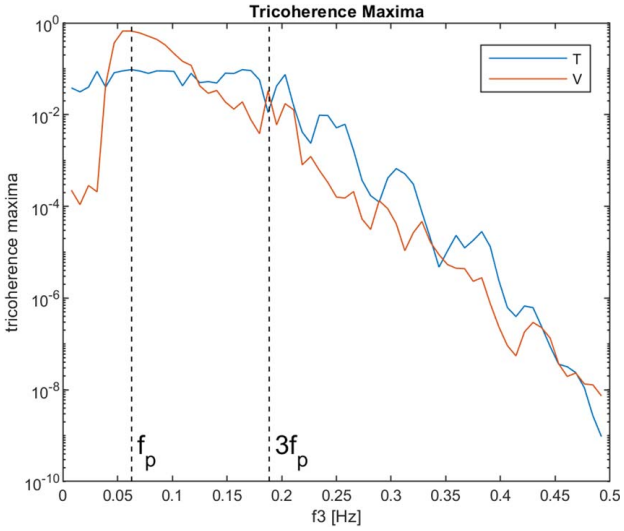

Fig. 9 f_3 slice maxima for the T and V-tricoherence estimates, for the HOS4 signal (Table 2)

model runs to order 5 might better indicate the performance of the trispectrum in a real sea state. Table 2 illustrates the unidirectional sea-state conditions that were simulated using the HOS model.

The four simulations with infinite water depth progress from $H_s =$ 5 m, through to $H_s = 15$ m, and so represent sea states of low to high steepness, in which the respective sea states are expected to be near linear (HOS1) to highly nonlinear (HOS4). The finite depth simulations represent sea states that are expected to be highly nonlinear but being in shallow water ($k_p d \approx 1$ and 2 for the HOS5 and HOS6 cases, respectively), a larger contribution of third-order bound terms are expected. We give focus in this paper to the analysis of the HOS4 and HOS5 records, which are expected to emphasize resonance and bound third-order interactions, respectively.

The f_3 axis slice maxima for the two tricoherence definitions are given in Fig. 9, for the HOS4 record. The plot shows high values of the V-tricoherence in the vicinity of the peak frequency, while the T-tricoherence does not show any significant values. Following findings for the sine wave above and that the tricoherences were not found to be significantly different from those obtained for HOS1, this result suggests that four-wave interactions of the type $f_4 = f_1 + f_2 + f_3$ are not strong or not active, but those of the type $f_1 + f_2 = f_3 + f_4$ may be active.

The trispectrum slices for $f_3 = f_p$ for the T- and V-tricoherence estimates are given in Figs. 10 and 11, respectively—f_p is the peak frequency of the power spectrum and is the frequency about which the V-tricoherence attains its largest values. The T-tricoherence has increased levels around f_p, but they are low (<0.1) and diffused over a relatively broad frequency range. In contrast to this, the V-tricoherence (Fig. 11) has significant values around f_p and is sharply focused about f_p.

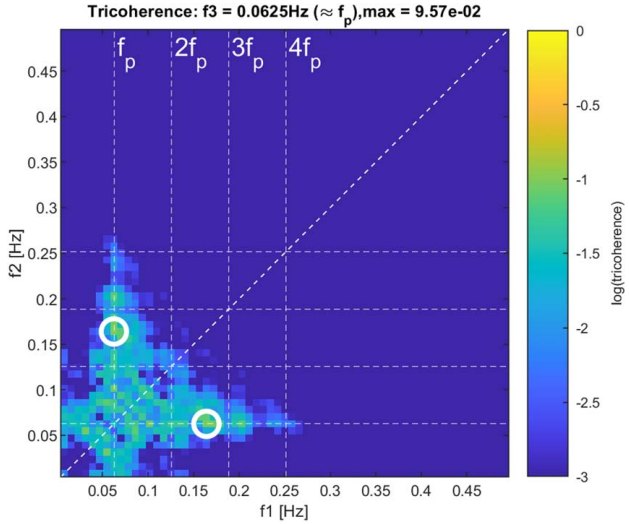

Fig. 10 T-tricoherence slice at $f_3 = f_p$ for the HOS4 signal

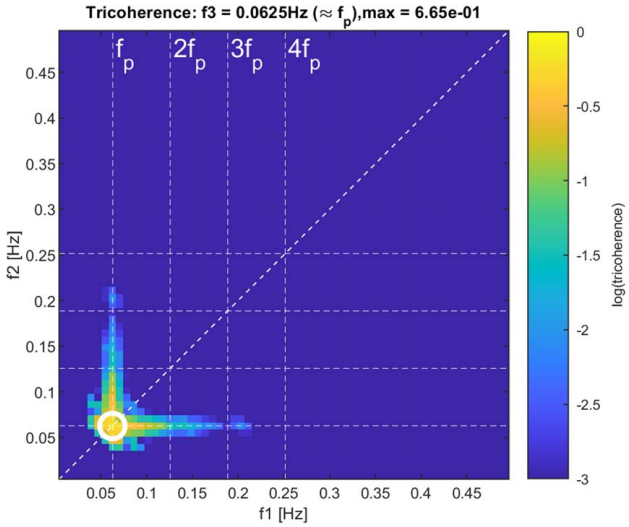

Fig. 11 V-tricoherence slice at $f_3 = f_p$ for the HOS4 signal

The f_3 axis slice maxima for the two tricoherence definitions for the HOS5 record are given in Fig. 12. The tricoherence curves are very similar to those for the HOS4 signal (Fig. 9), but with indications of slightly higher T-tricoherence values at low frequency (≈0.025 Hz), perhaps reflecting the presence of third-order difference frequency effects.

Laboratory Data

The laboratory record considered here was taken from experiments carried out at the MARINTEK Ocean Basin in Trondheim, Norway. The Basin has a water surface area of 50 m by 70 m with a variable depth of up to 10 m. The Basin is capable of producing multi-directional waves up to 0.4 m high at periods above 0.6 s. The particular record presented here is a combination of two irregular waves one with a peak enhancement parameter of 6 and the other 3. The combined significant wave height is 0.058 m, and the peak period of both irregular waves is 1 s. The water depth was 3 m [19].

The f_3 axis slice maxima for the two tricoherence definitions are given in Fig. 13. These curves are similar to those for the HOS spectra, with similar peak values, suggesting similar

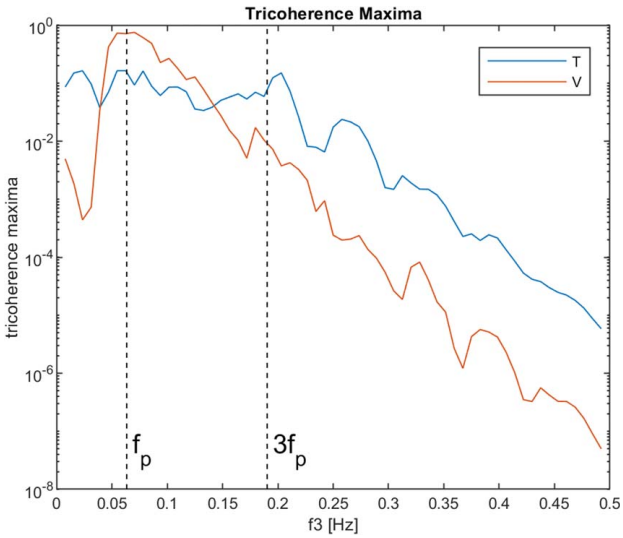

Fig. 12 f_3 slice maxima for the T and V-tricoherence estimates, for the HOS5 signal (Table 2)

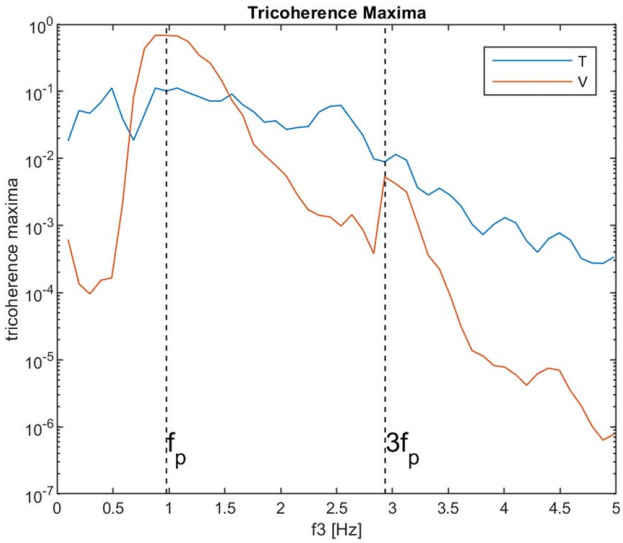

Fig. 13 f_3 slice maxima for the T and V-tricoherence estimates, for the laboratory signal

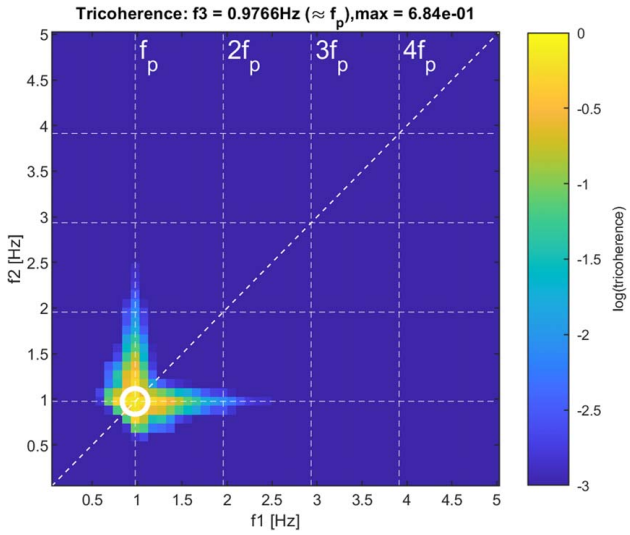

Fig. 14 V-tricoherence slice at $f_3 = f_p$ for the laboratory signal

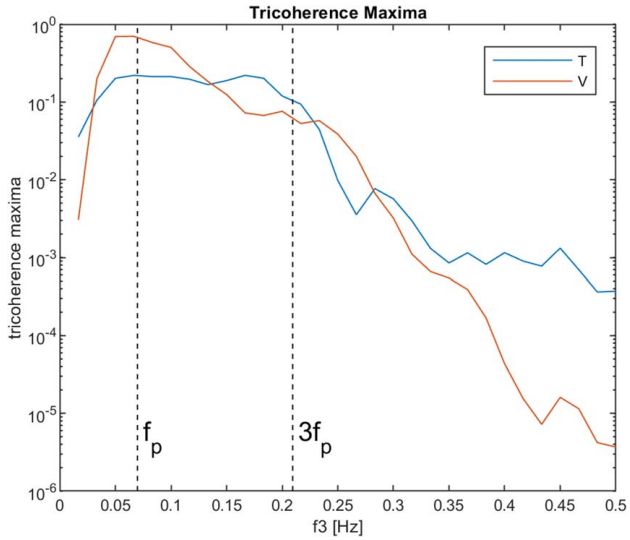

Fig. 15 f_3 slice maxima for the T and V-tricoherence estimates, for the Draupner wave record signal

interpretation—i.e., possibly four-wave interactions of the type where $f_1+f_2=f_3+f_4$, but not of the type $f_4=f_1+f_2+f_3$ that are phase-locked. The peak in the V-tricoherence at approximately $3f_p$ is notable, but with a peak value of around 0.01, it must be considered insignificant.

The f_3 axis slice images are similar to those for the HOS spectra; that for the V-tricoherence at $f_3 \approx f_p$ is given in Fig. 14, for example.

Draupner Wave Record

The final record that we consider is a field measurement recorded at the Draupner platform on Jan. 1, 1995. This record includes the unusually high crest event [20] that has received much attention. The Draupner location is in the North Sea where the water depth is 70 m. The wave measurements were made with a laser wave sensor.

The f_3 axis slice maxima for the two tricoherence definitions are given in Fig. 15. These curves are similar to those for the HOS and laboratory spectra, with similar peak values, although the maximum T-tricoherence value is approximately twice those of the HOS and laboratory maxima but still remains effectively insignificant. Thus, a similar interpretation begs—i.e., there is evidence of four-wave interactions of the type where $f_1+f_2=f_3+f_4$, but not of the type $f_4=f_1+f_2+f_3$ that are phase-locked.

Although not substantially different from the HOS and laboratory examples, we provide f_3 axis slice images for the T-tricoherence in Fig. 16 and V-tricoherence in Fig. 17 for $f_3 \approx f_p$ on account of the historical interest in the Draupner wave record and because we believe this is the first example of trispectral analysis of this record to be published. The images in these two figures have a lower resolution than the earlier examples, due to the lower sampling frequency of the Draupner measurements and our objective to reduce sampling variability in the estimates as far as practical. The images in Figs. 16 and 17 are qualitatively similar to the earlier examples, when consideration is given to the different resolutions involved.

Discussion

It might be expected that trispectra are limited to identifying only the class of four-wave interactions that are phase locked

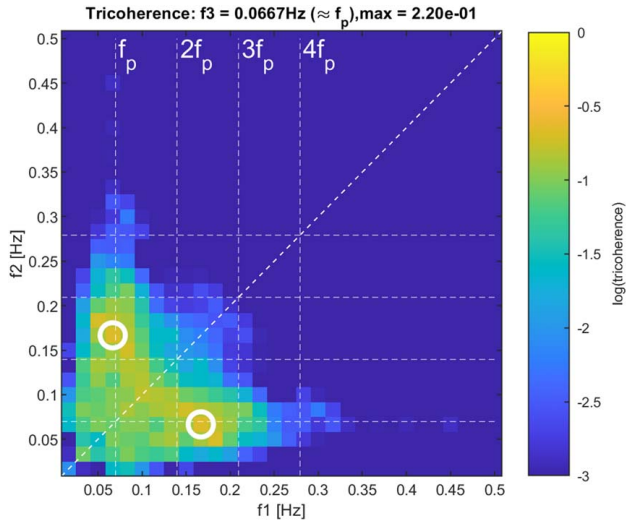

Fig. 16 T-tricoherence slice at $f_3 = f_p$ for the Draupner wave record signal

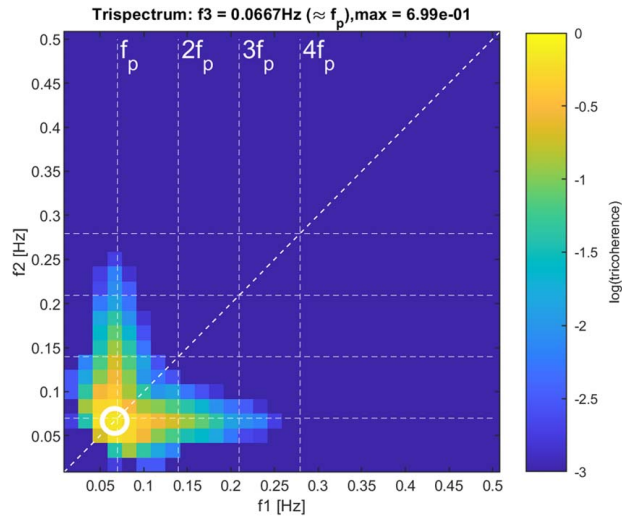

Fig. 17 V-tricoherence slice at $f_3 = f_p$ for the Draupner wave record signal

(see Appendix), thus providing no information on resonant interactions. However, the analysis reported here indicates that the application of both the T- and V-trispectral analyses may allow the possibility to assess whether or not four-wave interactions are phase-locked or not. This remains to be substantiated. For example, the Zakharov equation provides a Hamiltonian formulation for the evolution of the surface elevation. Using this formulation, it is possible to determine contributions at various orders of nonlinearity and from different sources, i.e., bound and resonant wave–wave interactions; this should provide an ideal testbed for trispectral analysis methods.

By definition, the V-tricoherence will indicate large values whenever the condition $f_1 + f_2 = f_3 + f_4$ is satisfied. For example, high values of V-tricoherence will occur when $f_1 = f_3$ and $f_2 = f_4$ (or $f_1 = f_4$ and $f_2 = f_3$) irrespective of whether four-wave interactions are active or not; the case when $f_1 = f_2 = f_3 = f_4 = f_p$ is a particularly relevant case in this respect, given the high V-tricoherence values we observed in the vicinity of the peak frequency in our results. The trivial solutions result from interactions between two pairs of components but not necessarily all four components together. Apparently, the trivial solutions correspond to events where interactions between components can be divided into groups that are statistically independent of each other and can be avoided by considering the cumulant-based trispectrum rather than the moment-based trispectrum [21]. Dalle Molle and Hinich [22] provide a good description of the difference between cumulant-based and moment-based trispectra. It is clear from the definition of the trispectrum that it strongly depends on the amplitudes of the Fourier components involved. Kravtchenko-Berejnoi et al. [21] suggest using the normalization of Brillinger [4] to obtain explicit information about the contribution of wave-wave interaction to the power of a certain oscillation. We are currently investigating the Kravtchenko-Berejnoi et al. [21] approach, and preliminary results of f_3 slice maxima applied to the HOS5 record (Table 2) and to the Draupner record are given in Figs. 18 and 19, respectively. The f_3 slice maxima corresponding to the Kravtchenko-Berejnoi et al. [21] tricoherence definition is the line labelled "K" in each plot, while those for the T- and V-tricoherences are the same as in Figs. 12 and 15. The plots show reduced K-tricoherence levels by comparison with the V-tricoherence levels in the vicinity of the spectral peak, substantially so in the case of the Draupner records, perhaps indicating removal of the contribution from the trivial solutions. The plots also show increased K-tricoherence levels by comparison with the V-tricoherence levels in the region around $3f_p$, and also at higher frequencies in the case of the Draupner records.

We have yet to incorporate uncertainty statistics, such as bias and variance, of our estimates; but these are well documented in the literature (see for example, Ref. [9] and it is our intention to include these in the form of error bars or noise floor levels, as appropriate in the various graphical presentations. Similarly, we intend to improve the clarity of our frequency-slice images by removing the redundant subdomains of the tricoherence functions, such as the region where $f_2 > f_1$.

Bispectra and trispectra provide representations of higher-order effects in sea states, in the Fourier sense. That is, analysis and interpretation is based on the record duration of the Fourier transform. Thus, short-term effects, such as localized nonlinear effects, are effectively averaged together with the rest of the record, which may be mostly linear. Accordingly, important highly nonlinear events will be watered down and may even be missed. Attempts to overcome this, at least in the case of bispectral analysis, by incorporating it in a wavelet approach have been shown to have some success in identifying nonlinear events in water wave records [23,24] and in other phenomena (van Milligen et al. [25–27]).

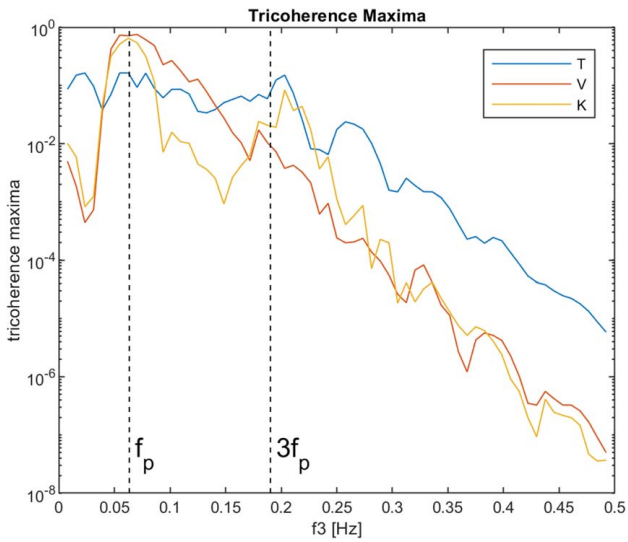

Fig. 18 f_3 slice maxima for the T and V-tricoherence estimates, for the HOS5 signal (Table 2), as in Fig. 12, plus those using the Kravtchenko-Berejnoi et al. [21] tricoherence definition (K)

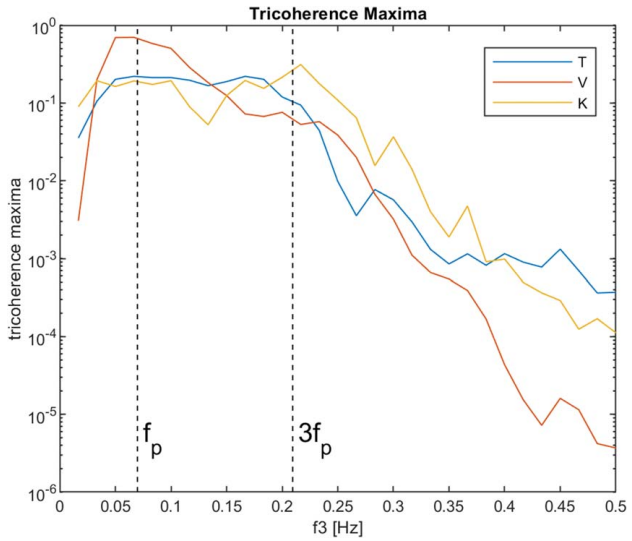

Fig. 19 f_3 slice maxima for the T and V-tricoherence estimates, for the Draupner signal, as in Fig. 15, plus those using the Kravtchenko-Berejnoi et al. [21] tricoherence definition (K)

It remains to be seen whether a wavelet approach can be extended to the incorporation of trispectra in wavelet analysis, to produce additional insight.

Finally, we note the application of the nonlinear Fourier analysis (NLFA) method [28], which provides (perhaps a superior) alternative to higher-order spectra that are based on conventional Fourier analysis, to investigate nonlinear effects in data sets. An example of the application of the NLFA on wave data is given by Osborne et al. [29]. Osborne et al. [29] remark that distinguishing characteristic of the NLFA method is its ability to spectrally decompose a time-series into its nonlinear coherent structures (Stokes waves and breathers) rather than just sine waves. This is done by the implementation of multidimensional, quasiperiodic Fourier series, rather than ordinary Fourier series.

Irrespective of the method, the ability to detect the presence of higher-order effects in time-series will enable key time-series realizations to be identified in engineering studies involving both physical and numerical model time-domain simulations. This will enable focus to be given to conditions likely to produce extreme crests and extreme loading on structures, and thereby assisting in the design of new or reanalysis of existing structures.

Conclusions

The T-tricoherence provides the capability to detect phase-locked four-wave interactions of the form $f_4 = f_1 + f_2 + f_3$, that is where three waves interact to force a bound fourth component. However, our estimates of the T-tricoherence on nonlinear wave simulations, and measured laboratory and field (Draupner) records did not indicate significant four-wave interactions of this type. While this result is expected for deep-water cases, we might have expected larger T-tricoherence values for the HOS5 (Table 2) case, for which $k_p d \approx 1$ and a significant contribution from third-order bound terms is expected in the signal.

Estimates of V-tricoherence produce high values at frequency triplets that correspond to high Fourier amplitudes. It is not possible to conclude whether these indicate the occurrence of actual four-wave interactions of the type $f_1 + f_2 = f_3 + f_4$, or whether they simply indicate combinations of independent pairs of Fourier components that happen to satisfy the frequency relationship. It is likely though that these four-wave interactions are present, in some of the sea states we investigated. We are currently investigating alternative tricoherence estimators to differentiate between these two possibilities or to exclude contributions from trivial combinations in the moment estimates.

Conflict of Interest

There are no conflicts of interest.

Appendix

Introduction. Consider a time-series $x(t) = \sum_{j=1}^{4} \cos(\omega_j^o t + \phi_j^o)$, for $t \in (-\infty, \infty)$, for real angular frequencies $\{\omega_j^o\}$ and phases $\{\phi_j^o\}$. The Fourier transform of $\exp(i\omega_j^o t)$ is given by $2\pi\delta(\omega - \omega_j^o)$ for $\omega \in (-\infty, \infty)$. Then it is straightforward to calculate the Fourier transform of $x(t)$ to be

$$X(\omega) = \sum_{j=1}^{4} \int_{-\infty}^{\infty} \cos(\omega_j^o t + \phi_j^o) e^{-i\omega t} dt$$

$$= \pi \sum_{j=1}^{4} e^{i\phi_j^o} \delta(\omega - \omega_j^o) + e^{-i\phi_j^o} \delta(\omega + \omega_j^o)$$

Using this result, it is relatively straightforward to calculate the values of different trispectral estimators in closed-form. It is also possible to calculate the statistical properties of trispectrum and tricoherence estimators for more general Gaussian series (with random Gaussian coefficients), as discussed in the full paper accompanying this work. Here, we restrict attention to the simplest useful cases to motivate thinking as clearly as possible.

T-trispectrum. For arbitrary angular frequencies $\{\omega_j\}$, we assume that $T(\omega_1, \omega_2, \omega_3) = X(\omega_1)X(\omega_2)X(\omega_3)X^*(\omega_1 + \omega_2 + \omega_3)$. Now we set $\omega_4^o = \omega_1^o + \omega_2^o + \omega_3^o$ for our time-series simulation above. We then see that

$$T(\omega_1^o, \omega_2^o, \omega_3^o) = \pi^4 e^{i(\phi_1^o + \phi_2^o + \phi_3^o - \phi_4^o)}$$

Fixed phases: For fixed values of $\{\phi_j^o\}$, it is obvious that the value of $T(\omega_1^o, \omega_2^o, \omega_3^o)$ will be nonzero and complex. In particular, $T(\omega_1^o, \omega_2^o, \omega_3^o)$ will be real only when $\phi_1 + \phi_2 + \phi_3 - \phi_4 = 2\pi n$, for $n = 0, \pm 1, \pm 2, \ldots$ That is, when phases are coupled as specified, the trispectrum is real.

Multiple realizations with random phases: If we assume that each ϕ_j is uniformly distributed on $[0, 2\pi)$, and that we have n occurrences $\{x_k(t)\}$ of $x(t)$ corresponding to different random draws of the phases, and corresponding estimates $\{T_k(\omega_1^o, \omega_2^o, \omega_3^o)\}$, then since $\int_0^{2\pi} e^{i\phi} d\phi = 0$, we will have $E[T(\omega_1^o, \omega_2^o, \omega_3^o)] = \left(\frac{1}{n}\right) \times \sum_k T_k(\omega_1^o, \omega_2^o, \omega_3^o) = 0$. That is, for multiple intervals of time-series with random phases, the expected trispectrum is zero. Note however if we take the absolute values of trispectra, that $E[|T(\omega_1^o, \omega_2^o, \omega_3^o)|] = \left(\frac{1}{n}\right) \sum_k |T_k(\omega_1^o, \omega_2^o, \omega_3^o)| = \pi^4$.

V-trispectrum. Suppose now that we assume that $V(\omega_1, \omega_2, \omega_3) = X(\omega_1)\, X(\omega_2)\, X^*(\omega_3)\, X^*(\omega_1 + \omega_2 - \omega_3)$, and that we set $\omega_4^o = \omega_1^o + \omega_2^o - \omega_3^o$ in the original time-series simulation, corresponding to the expected ocean wave 4-wave interaction. With this setting, we see that

$$V(\omega_1^o, \omega_2^o, \omega_3^o) = \pi^4 e^{i(\phi_1^o + \phi_2^o - \phi_3^o - \phi_4^o)}$$

In this situation, for fixed phases $\{\phi_j^o\}$, $V(\omega_1^o, \omega_2^o, \omega_3^o)$ will be complex unless $\phi_1^o + \phi_2^o - \phi_3^o - \phi_4^o = 2\pi n$, for $n = 0, \pm 1, \pm 2, \ldots$ for which $V(\omega_1^o, \omega_2^o, \omega_3^o) = \pi^4$. For multiple realizations of time-series with random phases, the expected value $E[V(\omega_1^o, \omega_2^o, \omega_3^o)] = 0$; but again, as for the T-trispectrum, we note the effect of taking absolute values.

In the Section entitled "Tricoherence of sinusoids" in the main text, we consider time-series of the form $y(t) = x(t) + \alpha(t)$ where $\alpha(t)$ is additive Gaussian (white) noise. The Fourier transform of $\alpha(t)$ is a constant at all frequencies by definition: $A(\omega) = \kappa$. This means that numerous trivial combinations of frequencies will always yield nonzero values of V-trispectrum. For instance, for $j = 1, 2, 3, 4$ and any ω_2

$$V(\omega_j^o, \omega_2, \omega_j^o) = |(X + A)(\omega_j^o)|^2 |(X + A)(\omega_2)|^2 \approx \pi^2 \kappa^2$$

if $\pi \gg \kappa > 0$. This occurs regardless of phase specifications (since phase relationships are also trivially satisfied in such cases). These trivial combinations do not occur for the T-trispectrum.

References

[1] Barber, N. F., Ursell, F., Darbyshire, J., and Tucker, M. J., 1946, "A Frequency Analyser Used in the Study of Ocean Waves," Nature, **158**(4010), pp. 329–332.

[2] Pierson, W. J., and Marks, W., 1952, "The Power Spectrum Analysis of Ocean Wave Record," Trans. Am. Geophys. Union, **33**(6), pp. 834–844.

[3] Tukey, J. W., 1949, "The Sampling Theory of Power Spectrum Estimates," Symposium on Applications of Autocorrelation Analysis to Physical Problems, NAVEXOS-0-735, Office of Naval Research.

[4] Brillinger, D., 1965, "An Introduction to Polyspectra," Ann. Math. Stat., **36**(5), pp. 1351–1374.

[5] Hasselmann, K., Munk, W., and McDonald, G., 1963, "Bispectra of Ocean Waves," *Time Series Analysis*, M. Rosenblatt, ed., Wiley, NY, pp. 125–139.

[6] Elgar, S., and Guza, R. T., 1985, "Observations of Bispectra of Shoaling Surface Gravity Waves," J. Fluid Mech., **161**, pp. 425–448.

[7] Cherneva, Z., and Guedes Soares, C., 2007, "Estimation of the Bispectra and Phase Distribution of Storm Sea States With Abnormal Waves," Ocean Eng., **34**(14–15), pp. 2009–2010.

[8] Toffoli, A., Onorato, M., Babanin, A. V., Bitner-Gregersen, E., Osborne, A. R., and Monbaliu, J., 2007, "Second-order Theory and Set-up in Surface Gravity Waves: A Comparison With Experimental Data," J. Phys. Ocean., **37**(11), pp. 2726–2739.

[9] Chandran, V., Elgar, S., and Vanhoff, B., 1994, "Statistics of Tricoherence," IEEE Trans. Signal Process., **42**(12), pp. 3430–3440.

[10] Elgar, S., Herbers, T. H. C., Chandran, V., and Guza, R. T., 1995, "Higher-order Spectral Analysis of Nonlinear Ocean Surface Gravity Waves," J. Geophys. Res., **100**(C3), pp. 4977–4983.

[11] Aubourg, Q., Campagne, A., Peureux, C., Ardhuin, F., Sommeria, J., Viboud, S., and Mordant, N., 2017, "Three-wave and Four-Wave Interactions in Gravity Wave Turbulence," Phys. Rev. Fluids, **2**(11), p. 114802.

[12] Haubrich, R. A., 1965, "Earth Noise, 5 to 500 Millicycles per Second 1," J. Geophys. Res., **70**(6), pp. 1415–1427.

[13] Kim, Y. C., and Powers, E. J., 1979, "Digital Bispectral Analysis and Its Applications to Nonlinear Wave Interactions," IEEE Trans. Plasma Sci., **7**(2), pp. 120–131.

[14] Hinich, M. J., and Wolinsky, M., 2005, "Normalizing Bispectra," J. Stat. Plann. Inference, **130**(1–2), pp. 405–411.

[15] Welch, P. D., 1967, "The Use of Fast Fourier Transform for the Estimation of Power Spectra: A Method Based on Time Averaging Over Short, Modified Periodograms," IEEE Trans. Audio Electroacoust., **15**(2), pp. 70–73.

[16] Harris, F. J., 1978, "On the Use of Windows for Harmonic Analysis With the Discrete Fourier Transform," Proc. IEEE, **66**(1), pp. 51–83.

[17] Ducrozet, G., Bingham, H. B., Engsig-Karup, A. P., Bonnefoy, F., and Ferrant, P., 2012, "A Comparative Study of Two Fast Nonlinear Free-Surface Water Wave Models," Int. J. Numer. Methods Fluids, **69**(11), pp. 1818–1834.

[18] Ducrozet, G., Bonnefoy, F., Le Touzé, D., and Ferrant, P., 2016, "HOS-ocean: Open-Source Solver for Nonlinear Waves in Open Ocean Based on High-Order Spectral Method," Comput. Phys. Commun., **203**, pp. 245–254.

[19] Luxmoore, J. F., Ilic, S., and Mori, N., 2019, "On Kurtosis and Extreme Waves in Crossing Directional Seas: A Laboratory Experiment," J. Fluid Mech., **876**, pp. 792–817.

[20] Haver, S., and Andersen, O. J., 2000, "Freak Waves—Rare Realizations of a Typical Population or Typical Realizations of a Rare Population?," Proceedings of ISOPE'2000, Seattle, WA, June, pp. 123–130.

[21] Kravtchenko-Berejnoi, V., Lefeuvre, F., Krasnossel'skikh, V., and Lagoutte, D., 1995, "On the Use of Tricoherent Analysis to Detect Non-Linear Wave-Wave Interactions," Signal Process., **42**(3), pp. 291–309.

[22] Dalle Molle, J. W., and Hinich, M. J., 1995, "Trispectral Analysis of Stationary Random Time Series," J. Acoust. Soc. Am., **97**(5), pp. 2963–2978.

[23] Ewans, K. C., and Buchner, B., 2008, "Wavelet Analysis of an Extreme Wave in a Model Basin," Proceedings of 27th International Conference on Offshore Mechanics and Arctic Engineering, Estoril, Portugal, June 15–19.

[24] Dong, G., Ma, Y., Perlin, M., Ma, X., Yu, B., and Xu, J., 2008, "Experimental Study of Wave-Wave Nonlinear Interactions Using the Wavelet-Based Bicoherence," Coastal Eng., **55**(9), pp. 741–752.

[25] van Milligen, B. P., Sánchez, E., Estrada, T., Hidalgo, C., and Brañas, B., 1995, "Wavelet Bicoherence: A New Turbulence Analysis Tool," Phys. Plasmas, **2**(8), pp. 3017–3032.

[26] Larsen, Y., and Hanssen, A., 2000, "Wavelet-polyspectra: Analysis of Non-Stationary and Non-Gaussian/Non-Linear Signals," Proceedings of the Tenth IEEE Workshop on Statistical Signal and Array Processing, Pocono Manor, Aug. 14–16, pp. 539–543.

[27] Schulte, J. A., 2016, "Wavelet Analysis for Non-Stationary, Nonlinear Time Series," Nonlinear Process. Geophys., **23**(4), pp. 257–267.

[28] Osborne, A. R., 2010, *Nonlinear Ocean Waves and the Inverse Scattering Transform*, Academic Press, Boston.

[29] Osborne, A. R., Resio, D., Costa, A., Ponce de Leon, S., and Chirivi, E., 2018, "Highly Nonlinear Wind Waves in Currituck Sound: Dense Breather Turbulence in Random Ocean Waves," Ocean Dyn., pp. 187–219.